NANO LETTERS

LETTER

pubs.acs.org/NanoLett

Light Propagation in Curved Silver Nanowire Plasmonic Waveguides

Wenhui Wang,[†,‡] Qing Yang,[‡,§] Fengru Fan,[‡] Hongxing Xu,[†,*] and Zhong Lin Wang*[,‡]

[†]Beijing National Laboratory for Condensed Matter Physics and Institute of Physics, Chinese Academy of Sciences, Box 603-146, 100190, Beijing, China

[‡]School of Materials Science and Engineering, Georgia Institute of Technology, Atlanta, Georgia, 30332, United States

[§]Department of Optical Engineering, Zhejiang University, Hangzhou 310027, China

Supporting Information

ABSTRACT: Plasmonic waveguides made of metal nanowires (NWs) possess significant potential for applications in integrated photonic and electronic devices. Energy loss induced by bending of a NW during light propagation is critical in affecting its performance as a plasmonic waveguide. We report the characterization of the pure bending loss in curved crystalline silver NW plasmonic waveguides by decoupling the energy loss caused by bending and propagation. The energy attenuation coefficiency due purely to bending was also determined, which exhibited an exponential relationship with the bending radius. Finite-difference-time-domain (FDTD) methods were utilized for theoretical simulations, which matched the experimental results well.

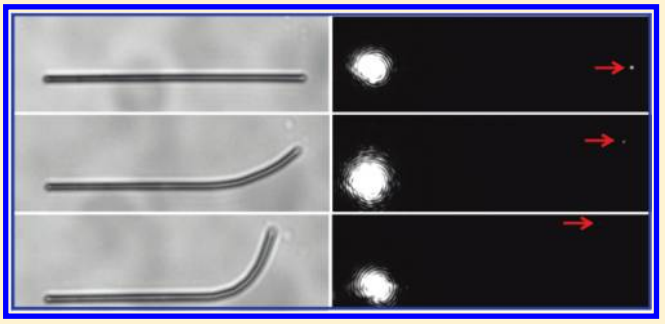

KEYWORDS: Silver nanowire, plasmonic waveguide, bending loss, plasmonic circuit, plasmon propagation, bending radius

Surface plasmon polaritons (SPP) were first theoretically proposed in 1957 based on dielectric excitation of a thin metal film by a charged particle.[1] The excitation of SPPs was extensively studied in 1980−1990s using electron energy loss spectroscopy (EELS) by utilizing a fine electron probe in a scanning transmission electron microscope (STEM),[2] which excites nanoparticles/nanotubes of various geometrical shapes.[3,4] The dielectric excitation theory for plasmons in EELS is well established, which not only can predict the plasmon energies, but also can give quantitative results about the excitation probability as a function of the electron impact factor and nanoparticle shape and size.[5] However, due to the limited energy resolution provided by EELS in STEM in the order of 0.5−1 eV, the SPPs studied by EELS typically have energy of a few electronvolts.

Recently, using a fine focused laser beam, SPPs with energies from visible to near-infrared range have been studied for a range of nanomaterials, such as nanowires (NWs), which can serve as waveguides for plasmon propagation, and have the advantage of localizing the electromagnetic energy in nanoscale regions that are much smaller than the wavelengths of light in the material.[6,7] Nanowire plasmonic waveguides also offer significant potential for the miniaturization of optical signal processing/sensing devices at the subwavelength scale and the integration of photonic circuits with external devices to overcome the fundamental data transmission rates and bandwidth limitations in conventional electrical technology.[8,9] As an efficient method to manipulate light at the nanometer scale, plasmonic waveguiding has been extensively investigated[10−18] and has enabled a wide range of applications including plasmonic routers and multiplexers,[18] Bragg mirrors,[19] interferometers,[20] and electro-optic devices.[21]

The capability of plasmonic waveguides to localize the electromagnetic energy in nanoscale regions arises from the hybrid nature of SPP, which is an electromagnetic wave coupled to charge oscillation at the metal−dielectric interface. The electromagnetic field perpendicular to the interface decays exponentially with distance from the surface. SPP can be laterally confined below the diffraction limit and propagate over distances exceeding tens of micrometers in silver, which is the material with the lowest loss in visible spectrum.[7] Various types of metallic nanostructures such as nanoparticle chains,[11,22] thin metal films,[23] metal slits,[24] grooves,[25] and nanowires[26−30] have been widely investigated to guide SPP modes for developing unique nanophotonic systems and efficient delivery of light energy at nanoscale as potential nanophotonic devices.

To design SPP-based devices, it is essential to study the energy attenuation process in the plasmonic waveguides associated with SPP propagation, such as intrinsic ohmic loss owing to absorption in the metal[7,12,31] and radiative energy loss resulting from discontinuities or continuous bending of the waveguides. In particular, the bending loss is a critical factor limiting the performance of SPP modes as signal carriers in optical integrated devices. However, few studies have been conducted to investigate the bending loss in chemically synthesized nanowire waveguides due to the difficulty in achieving continuous bending. The majority of previous efforts have focused on structures such as metallic stripes,[32] wedges,[33] grooves,[25] splitters,[34] and sharp bends,[35−37]

Received: December 27, 2010
Revised: February 12, 2011
Published: March 16, 2011

which are fabricated by conventional lithography methods. These structures usually suffer severe scattering loss compared with chemically synthesized metal nanowires due to inevitable surface corrugations originating from the metal evaporation process and polycrystalline nature of these structures. The chemically synthesized metal NWs can drastically enhance SPP propagation distances and are promising candidates for applications such as interconnects in integrated optical and electronic circuits at nanoscale, due to advantages such as high crystallinity and smooth surfaces. Energy attenuation of propagating SPPs due to geometrical bending in chemically synthesized metal NWs, however, has yet to be elucidated. Here we present experimental and theoretical characterization of radiative loss of SPPs during the continuously in situ bending process of single chemically synthesized silver nanowires (Ag NWs). This continuous shape change of a Ag NW to control the bending radius at one end was realized by manipulating the NW using a tapered optical fiber.

The crystalline Ag NWs were synthesized using a two-step modified seed-mediated growth method,[38] yielding Ag NWs with diameters ranging from 550 to 800 nm and lengths from 20 to 50 μm (see Supporting Information Figure S1). The synthesized Ag NWs were purified via centrifugation in ethanol then deionized water for several cycles in each solvent. The obtained suspension solution of Ag NWs was then deposited onto a clean glass substrate for subsequent manipulation. Several different approaches have been developed for the excitation and characterization of SPP modes in metallic structures.[10,12,39−41] In the present work, a near-field coupling method was adopted for the efficient excitation of SPP in Ag NWs.[30,31] This method can be used to directly excite SPPs in the midsection of Ag NW where light cannot be coupled into the waveguides directly from free space.[17,42] Specifically, the guided photonic modes in a tapered optical fiber can be coupled to the plasmonic propagation modes in the Ag NW when the fiber and Ag NW are placed close enough to each other. The measurement of energy loss in the bent Ag NW was carried out by comparing the intensity of emission light at the bent end of Ag NW at different bending radii. Tapered optical fibers with a tip diameter of around 800 nm were fabricated from standard silica fiber (Thorlabs, SMF28) by a method reported elsewhere.[43] The position and contacting direction of the optical fiber can be precisely adjusted by a three-axis translation stage. Two types of laser sources, a He−Ne laser emitting at a wavelength of 633 nm and a laser diode emitting at 785 nm, the latter stabilized by the current controller (Thorlabs, LDC205c) and temperature controller (Thorlabs, TED200c), were used for exciting SPPs in the Ag NWs. The incident light was first coupled into a standard fiber (Thorlabs, P1-SMF28-FC) with a lens, then squeezed into the nanofiber through a fiber coupler, resulting in the quasi-circular-polarization guided modes (HE_{11} modes) with high-fractional evanescent fields.[44]

In our experiment, two tapered optical fibers were employed for different purposes: one for directing the excitation light into Ag NW and the other for applying a force to bend the NW. The natural adhesion of the Ag NW to the substrate is sufficient to hold one end of the nanowire in place while the other is manipulated with the fiber probe, but not so great as to prevent manipulation of the Ag NW. When excited at the unbent end of Ag NW, SPPs were propagating along the NW and partially scattered into free space at the bent end of the NW. The emission from the bent end of the NW was collected by a 50× objective (numerical aperture 0.55) and the optical image was recorded by a charge-coupled-device (CCD) camera mounted on the microscope (Nikon Eclipse Ti inverted microscope). The intensity of the emission was obtained by determining the maximum value in the emission spot from the optical image. The bending radius was directly measured from bright-field optical images obtained under wide-field illumination by a halogen lamp.

The propagation losses, including intrinsic ohmic loss arising from metal absorption as well as scattering loss owing to the variations of the metal surface morphology and fabrication imperfections in Ag NW are inevitable in plasmonic waveguides. Furthermore, the propagation losses may vary significantly from structure to structure. Therefore, to determine the bending loss in curved Ag NW waveguides, the propagation process in straight Ag NW needs to be characterized first and then decoupled from the effect of bending. For each measurement, the angle and position of the tapered optical fiber for coupling light into the Ag NW was carefully adjusted until the coupling was optimized with maximum emission light intensity at the bent end of Ag NW. A 785 nm laser was used for the excitation of SPPs in the Ag NW with diameter of 750 nm and length of 45 μm. By placing the light-coupling tapered optical fiber at different locations along the Ag NW, the propagation distance can be changed from 5 to 42 μm in step of 5 μm and the corresponding decrease in intensity of the emitted light with increasing propagation distance was observed. Selected optical images are shown in Figure 1a and the corresponding dark-field optical images are shown in Figure 1b. By plotting the measured emission light intensity at the output end of the Ag NW against varying propagation distances x (Figure 1c), the effective propagation length L_0, the length at which the light intensity decreases to $1/e$ of the initial value, can be determined by fitting the data to an exponential decay

$$I(x) = I_0 e^{-x/L_0} \quad (1)$$

where I_0 is the initial intensity coupled into the input end of the Ag NW. Then the propagation loss expressed in decibels (dB), $-10 \log(I/I_0)$, can be calculated and plotted as the red dotted line in Figure 1c. The propagation length is found to be $L_0 = 10.6$ μm (the distance that the corresponding energy loss is 4.3 dB) for SPP propagation using 785 nm laser excitation, corresponding to an attenuation coefficient $\alpha_0 = 1/L_0 = 0.094$ μm^{-1}. The propagation loss per unit length along the Ag NW is then 0.41 dB/μm and the total propagation loss along the 45 μm long nanowire is approximately 18.5 dB. In addition, the investigation of propagation loss has also been carried out in several other Ag NWs with different diameters and lengths and observed to range from 0.35 dB/μm to 0.48 dB/μm, which is comparable to previous results.[42,45] Although the propagation loss decreases as the diameter increases,[6] the small variation observed here in the measured propagation loss per unit length for the Ag NWs results from the uniform distribution in diameter of the Ag NWs investigated in this experiment (see Figure S1 in Supporting Information).

Bending loss occurring in the curved NW during bending is a radiative process that converts the energy from propagating modes to free radiation. This occurs because bending changes the momentum of k_{SPP}, and the changed part Δk_{SPP} should be compensated by the momentum of the light radiation. Bending radii ranging from 5 to 32 μm in a Ag NW with diameter of 750 nm and length of 45 μm was achieved by tapered optical fiber manipulation. The results in Figure 2a are selected optical images to demonstrate the continuous bending process in one Ag NW,

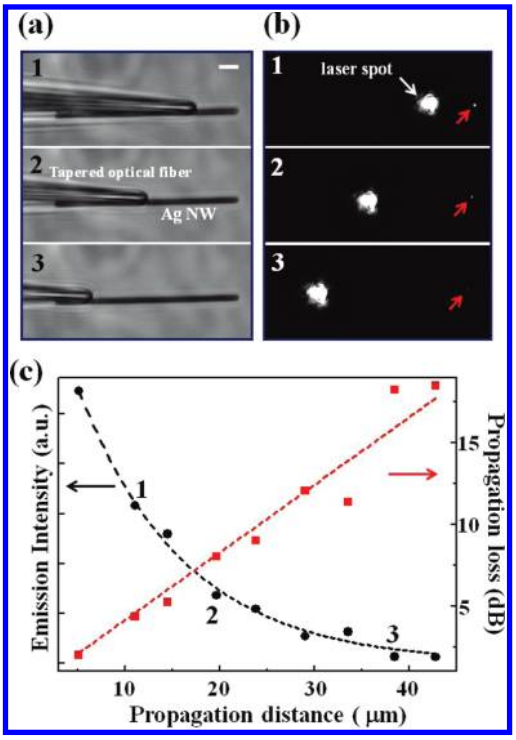

Figure 1. Measured propagation losses for varying distances along the Ag NW waveguide. (a) Bright-field optical images and (b) corresponding dark field optical images are obtained for the Ag NW with diameter of 750 nm and length of 45 μm. A 785 nm laser, directed by the tapered optical fiber (as indicated in inset (a) 2), is used for the excitation of SPPs in the Ag NW. The emitted light at the output end of Ag NW is shown in (b) 1, (b) 2, and (b) 3 as indicated by the red arrows, which corresponds to propagation distance of 11, 19, and 38 μm, respectively. The scale bar is 5 μm. (c) The intensity of emitted light at the output end of the Ag NW (black circles) and the corresponding propagation loss (red squares) for different propagation distances. The black dotted curve is the exponentially fitted emission intensity for different propagation distances. The red dotted line is the linearly fitted propagation loss in dB for varying distances along the Ag NW waveguide.

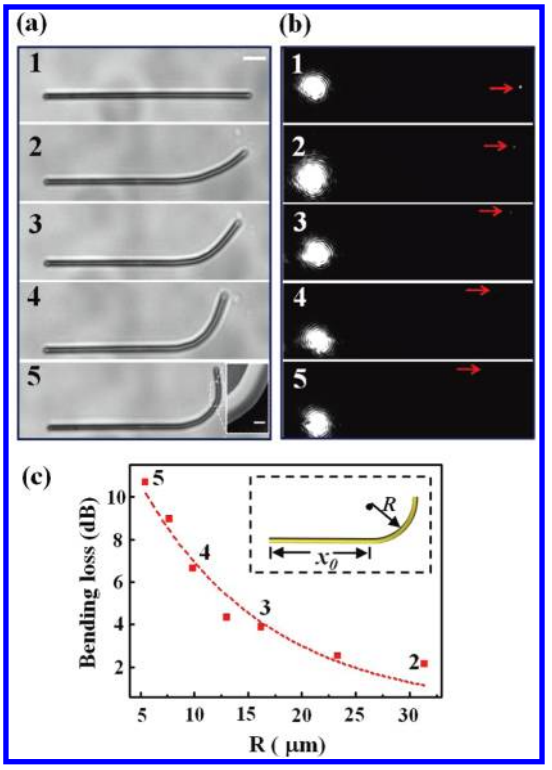

Figure 2. Measured bending loss for varying bending radii. (a) Images 1−5 are the selected bright-field optical images demonstrating the bending process of the Ag NW with diameter of 750 nm, length of 45 μm, and bending radii of ∞, 32, 16, 9, and 5 μm, respectively. The inset is the SEM image of the curved section with scale bar of 350 nm. (b) Images1−5 are the dark-field optical images for the corresponding bending process. The emitted light at the bent end of Ag NW are indicated by the red arrows and 785 nm laser is used for the excitation. The scale bar is 5 μm in (a) 1−5 and (b) 1−5. (c) Pure bending loss as a function of bending radius. The red curved line is the exponential fit to the bending loss in the Ag NW at certain bending radius, which is obtained by subtracting the propagation loss from the measurement of emitted light intensity in (b) 1−5. Inset: geometry of the bent wire. The length of the straight section is x_0, and the bending radius is R.

where the bending section of the Ag NW is smooth and no defects can be seen in the SEM image (inset in Figure 2a). The intensities of the emitted light at the bent end of the Ag NW for varying bending radius are measured in the dark-field optical images, recorded in situ during the bending process (Figure 2b). It can be clearly observed that the emitted light spot is dimer at the bent end of the Ag NW with decreasing bending radius when the incident laser intensity is kept constant (Figure 2b). In addition, there is no observable emission of light along the curved section of the Ag NW. Since the bending is smooth over a large length scale (tens of micrometers), the radiation is also spread over a large area and may therefore be too weak to be observed. It can be seen from the SEM image in the inset of Figure 2a-5 that no discernible deformation or cracking of the surface structure/morphology exists. The emission intensity can be directly obtained by determining the maximum value in the emission spot from the optical images in Figure 2b and thus the total energy loss in the Ag NW can be acquired.

As discussed previously, the propagation loss exists whenever SPP propagates along the plasmonic waveguides regardless its local curvature. The propagation loss along the entire Ag NW can be considered as a constant value (e.g., 18.5 dB in this Ag NW of length around 45 μm) during the bending process since the variation in the length of the Ag NW is insignificant. Consequently, the energy loss resulting purely from the bending process can be isolated by subtracting the propagation loss along the entire Ag NW from the total energy loss. This pure bending loss for the same Ag NW in Figure 2a plotted as the red dotted curve in Figure 2c, exhibits an exponential attenuation trend with increasing bending radius and achieves 11 dB when the bending radius decreases to 5 μm (Figure S2 in Supporting Information). The obvious dependency of bending loss on bending radius of Ag NW demonstrates that the emitting light intensity at the output end of bent Ag NW is sensitive to the shape deformation of NW, which has the potential applications such as stress sensor.

For the description of bending loss, the simplest reasonable assumption is that the emitted light intensity at the bent end of Ag NW still decays exponentially with the length of curved section but with a different attenuation coefficient, which varies when the bending radius changes.[37] The expression is therefore proposed as

$$I = I_0 e^{-l/L_0} e^{-\alpha(l - x_0)} \quad (2)$$

where I_0 is the initial input intensity, α is the parameter to depict

dx.doi.org/10.1021/nl104514m |Nano Lett. 2011, 11, 1603–1608

the energy attenuation per unit length around the bending section due to bending loss, l is the length of the Ag NW, x_0 represents the length of the straight segment as shown in the inset of Figure 2c. In the following calculation, x_0 is taken as a constant since the variation is small during the whole bending process, which is confirmed by the measurement from bright-field optical images. It is convenient to express the bending loss ρ in dB as

$$\rho = -10 \log e^{-\alpha(l - x_0)} = -10 \log \frac{I}{I_0} - \frac{10}{2.3}\left(\frac{l}{L_0}\right) \quad (3)$$

From Figure 2c, the shape of the bending loss ρ as a function of the bending radius R can be mathematically matched if the attenuation coefficient is a function of the form

$$\alpha \approx C_g e^{-\beta R} \quad (4)$$

where C_g and β are fitting parameters depending on the shape and optical properties of the nanowires.[37] Then the value of α at certain bending radius can be calculated and shown in Figure S3 (see Supporting Information). It can be observed that the energy attenuation coefficient α due to bending process exceeds that of the propagation loss if the bending radius is less than 10 μm, demonstrating that the bending loss plays an important part for the contribution of energy attenuation at small bending radius. This is important for the estimation of energy loss in the design of practical SPP-based photonic circuits.

The electric field intensity distributions calculated using the FDTD method are shown in Figure 3b (Lumerical FDTD solutions). The geometry of the Ag NW is modeled as a cylinder (diameter of 750 nm and length of 45 μm) on a glass substrate (refractive index 1.5) as shown in the schematic picture (Figure 3a). The electric field distribution in the straight segment of Ag NW is not shown in Figure 3b as it does not suffer deformation when Ag NW is curved. It can be observed that the attenuation of electric field in Figure 3b-2 (bending radius is 25 μm) is very close to that of the straight one shown in Figure 3b-1, and the intensity of electric field at the output end of Ag NW decreases compared to the original straight one (see insets in Figure 3b-1 and b-2). This difference is enhanced when the bending radius of Ag NW decreases as shown in Figure 3b-3 (bending radius is 10 μm). The electric field decays quickly along the bending section of Ag NW and a small portion of electric field distribution on the outside of the Ag NW is also observed, which thus results in the very weak intensity of electric field distribution at the output end of Ag NW (see the inset in Figure 3b-3). The corresponding calculated bending loss plotted as a function of bending radius in Figure 3c demonstrates that the bending loss increases when the bending radius decreases, which is consistent with the experimental observations. It should be, however, noted that the influence of strain-induced crystalline structure change on the bending loss, as well as the quantitative analysis of effect of the polarizations of guided light on the bending loss need to be addressed in theoretical and experimental work in the future.

The interaction between the surface charge oscillation and the electromagnetic field results in the momentum mismatch between SPP mode ($\hbar k_{spp}$) and a free space photon ($\hbar k_{photon}$). The mismatch in momentum, $\hbar\Delta k$, needs to be compensated via a scattering mechanism,[7] which can be realized at the sites of either discontinuity or defects where the symmetry in structure or geometry is broken and light can thus be coupled into propagating surface plasmon modes. Vice versa, plasmon modes can also be scattered in the form of photons at the output end of the NW.

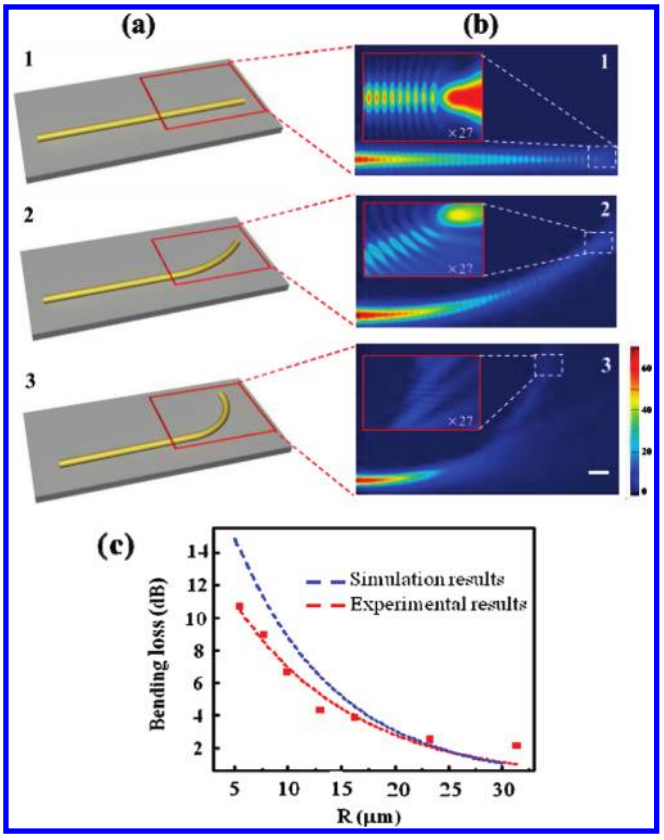

Figure 3. The calculated distribution of electric field intensity around a Ag NW by the FDTD method. (a) Schematics of a Ag NW when it is straight in (a) 1, and bent with bending radius of 25 μm in (a) 2 and 10 μm in (a) 3. (b) The calculated electric field distribution. The insets show the corresponding distribution of electric field intensity at the output end of Ag NW. The maximum intensity of color bar in the inset is 27 times lower than that of the color bar shown on the bottom. The scale bar is 1 μm. (c) The caculated bending loss as a function of bending radius (in blue). The observed experimental results as in Figure 2c are also shown for comparison (in red).

The above two scenarios have been observed experimentally and shown in Figures 2 and 4, respectively. In the case of Figure 2, the chemically synthesized Ag NW with smooth surface does not suffer observable bending-induced cracks or defects and only light emitted at the output end of Ag NW can be observed. On the contrary, defects or discontinuities such as cracks introduced during the bending process can result in the propagating plasmons, which are scattered into photons and observed as bright light emitted spots at these defective sites, as shown in Figure 4b. When there is no bending (Figure 4a-1) or the bending radius is large (Figure 4a-2), no defective deformations can be observed along the NW and the emitted light can only be seen at the output end of the NW (Figure 4b-1,2). When the bending radius gets smaller, on the other hand, sharp bends together with cracks and defective sites can form easily as revealed in SEM image (the inset of Figure 4a-3) and propagating SPPs can be significantly scattered by these symmetry breaking sites into free-space photons, observed as bright light spots and indicated by the red dotted circles (Figure 4b-3). This is in accordance with the phenomenon of radiation in NW with kinks reported previously.[26] The intensity of the right light spot is much weaker than the left one probably because a great majority of light has been scattered

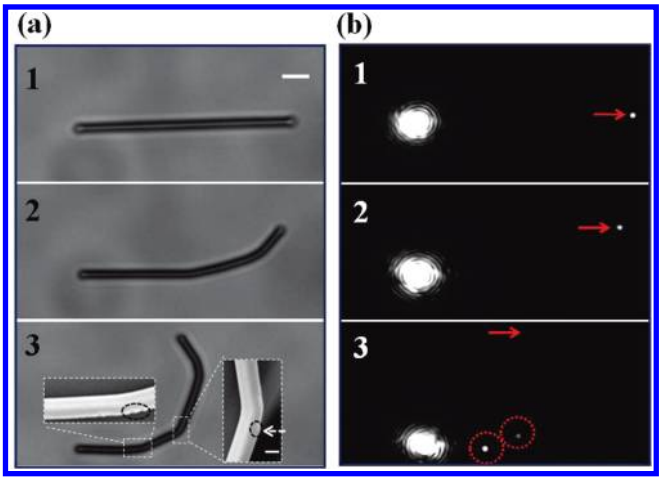

Figure 4. Effect of discontinuities and defects in the Ag NW on the propagation of SPPs. (a) Bright-field optical images demonstrating the bending process of the Ag NW with diameter of 800 nm and length of 40 μm. No observable fracture or defect can be seen in (a) 1 and (a) 2. In (a) 3, however, a fracture and a defect can be observed in the areas indicated by the white dotted lines. Insets are the SEM images with the scale bar of 500 nm. (b) Images 1−3 are the corresponding dark-field optical images. No bright spot can be seen along the Ag NW between the output and input ends in (b) 1 and (b) 2, while two bright emission spots appear at the defective sites of the Ag NW in (a) 3. The scale bar is 5 μm.

out by the left-hand defects when the propagating SPPs arrives and thus only a small portion of propagating SPPs exists in Ag NW before arriving the right-hand one.

Since a large amount of the propagating modes are scattered out into photons at these two positions, the emitted light at the end of Ag NW is weak compared to those in Figure 4b-1,2, as indicated by the red arrowheads. Therefore, SPP propagation upon abrupt discontinuities can be scattered significantly into free-space photons (Supporting Information Figure S4), compared with the situation that the symmetry is gently broken over large length scales, as previously demonstrated in Figure 2a and Figure 4a-2, where SPPs cannot be coupled out in an efficient manner and hence no observable emission of light can be seen. Unlike light emitted at the defective sites of the Ag NW that appears as bright spots (Figure 4b-3), the radiative loss along the smooth bending section is too weak to be directly recorded by CCD camera. To study the radiative loss in the curved Ag NW, it is essential to investigate the variation of emitted light intensity with varying bending radius including the initial straight Ag NW, which can be taken as the nanowire with infinite bending radius. The sharp bends, on the other hand, can be intentionally made to scatter the SPP modes into free space photons for the special purpose when SPPs are served as information carrier in the future integrated photonic circuits and devices.

The dependence of energy loss in bent Ag NW on other parameters such as the wavelength of excitation light and the diameter of the NW waveguide has also been investigated. The lasers with wavelength of 785 and 633 nm were used respectively for the excitation. More significant energy loss was observed for longer wavelength excitation at bending radius ranging from 5 to 32 μm as shown in Figure 5a. This is different from the propagation loss which tends to decrease in longer wavelength.[46] However, considering the relative bending radius R_{eff}, which is defined here as $R_{eff} = R/\lambda$, that is, 1.24 times larger for 633 nm than 785 nm, the energy loss versus R_{eff} is actually quite similar for different

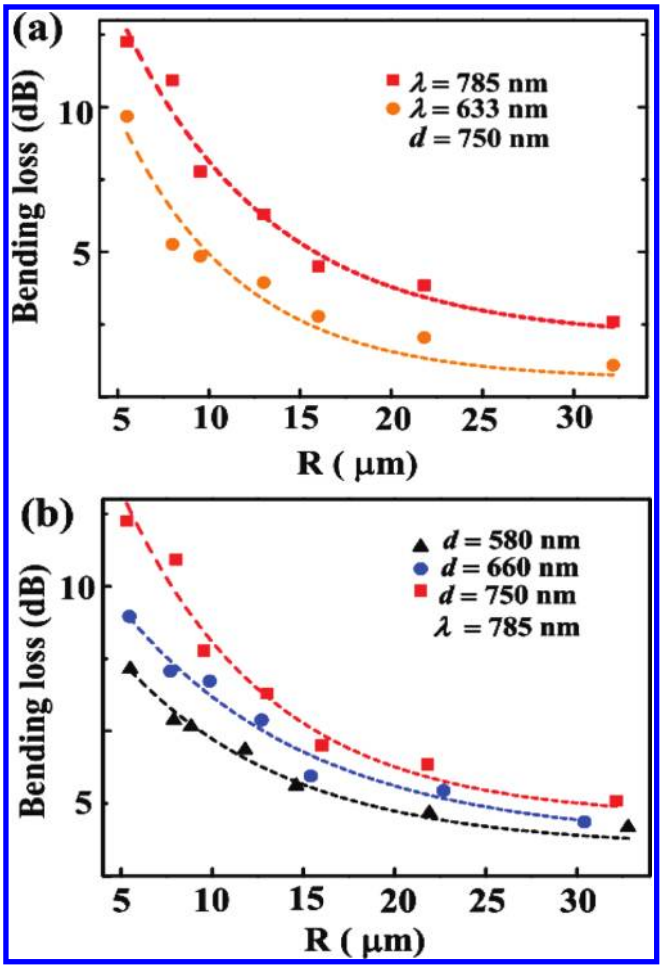

Figure 5. Dependence of pure bending loss on the wavelength of excitation light and the diameter of the Ag NW waveguides. (a) The pure bending loss in the Ag NW with a 785 nm laser and a 633 nm laser as the excitation source. The diameter of the Ag NW is 750 nm. (b) The pure bending loss in Ag NWs with a diameter of 580, 660, and 750 nm, respectively, when the 785 nm laser is used for excitation. Symbols represent the measured data and the dashed lines are the corresponding fits to the data as described in the text.

wavelengths (see Supporting Information Figure S5). This indicates that the bending loss for different wavelength of excitation laser in Ag NW follows such a scaling law.

It is also observed that the bending loss in curved Ag NW increases as the diameter of the NW becomes larger at fixed excitation wavelength and bending radius as shown in Figure 5b. Under the excitation of 785 nm laser, the bending loss is suppressed when the diameter of Ag NWs decreases from 750 to 580 nm for fixed bending radius. It is known that SPPs are excited and propagated in different modes in Ag NWs, and the higher-modes will possess increased portion when the diameter of NWs becomes larger. Since the momentum of higher order modes is closer to that of the emitted photons,[47] the thicker NW can serve more radiative loss than the thinner one as observed in Figure 5b. These experimental observations are well consistent with our simulation result (see Figure S6 in Supporting Information).

In conclusion, the bending loss of SPP propagation in Ag NW of bending radius ranging from 5 to 32 μm has been investigated. The precise control of the incident laser spot position enables us to obtain the propagation loss of SPP propagating in the Ag

dx.doi.org/10.1021/nl104514m |*Nano Lett.* 2011, 11, 1603–1608

NWs. FDTD method was utilized for simulating the SPP propagation in bent Ag NWs, and the simulation results agree well with the experimental results. The energy loss in a bent Ag NW is also influenced by the wavelength of the excitation laser and the diameter of the Ag NW. In addition, the effect of discontinuity and defects for the scattering of propagating SPPs modes from Ag NW waveguides to the free space light has been demonstrated. The quantitatively and qualitative investigation of bending loss in Ag NW waveguides is insightful for the future SPP-based photonic circuits and devices.

■ ASSOCIATED CONTENT

Supporting Information. Additional figures. This material is available free of charge via the Internet at http://pubs.acs.org.

■ AUTHOR INFORMATION

Corresponding Author
*E-mail: (Z.L.W.) zhong.wang@mse.gatech.edu; (H.X.X.) hxxu@iphy.ac.cn.

■ ACKNOWLEDGMENT

Research was supported by DARPA (HR0011-09-C-0142, Program manager, Dr. Daniel Wattendorf), Airforce, BES DOE (DE-FG02-07ER46394), NSF (DMS0706436, CMMI 0403671), National Institute For Materials, Japan (Agreement DTD 1 Jul. 2008), NSFC Grants (10625418 and 10874233), MOST Grants (2007CB936800 and 2009CB930700), the "Bairen Project" and the "Knowledge Innovation Project" of CAS under Grant KJCX2-EW-W04. The authors acknowledge valuable discussions with Dr. Yan Zhang, Shunping Zhang, Yurui Fang, Dr. Nathaniel K Grady, and Dr. Xin Guo and technical assistance from Ying Liu and Bin Hu. The authors also thank technical assistance from Amy Liu and Angus Fraser in Lumerical Solutions, Inc.

■ REFERENCES

(1) Ritchie, R. H. *Phys. Rev.* **1957**, *106* (5), 874–881.
(2) Batson, P. E. *Solid State Commun.* **1980**, *34* (6), 477–480.
(3) Wang, Z. L.; Cowley, J. M. *Ultramicroscopy* **1987**, *21* (1), 77–93.
(4) Yannouleas, C.; Bogachek, E. N.; Landman, U. *Phys. Rev. B* **1994**, *50* (11), 7977–7980.
(5) Wang, Z. L. *Micron* **1996**, *27* (3−4), 265–299.
(6) Gramotnev, D. K.; Bozhevolnyi, S. I. *Nat. Photonics* **2010**, *4* (2), 83–91.
(7) Barnes, W. L.; Dereux, A.; Ebbesen, T. W. *Nature* **2003**, *424* (6950), 824–830.
(8) Ozbay, E. *Science* **2006**, *311* (5758), 189–193.
(9) Engheta, N. *Science* **2007**, *317* (5845), 1698–1702.
(10) Pyayt, A. L.; Wiley, B.; Xia, Y. N.; Chen, A.; Dalton, L. *Nat Nanotechnol.* **2008**, *3* (11), 660–665.
(11) Maier, S. A.; Kik, P. G.; Atwater, H. A.; Meltzer, S.; Harel, E.; Koel, B. E.; Requicha, A. A. G. *Nat. Mater.* **2003**, *2* (4), 229–232.
(12) Ditlbacher, H.; Hohenau, A.; Wagner, D.; Kreibig, U.; Rogers, M.; Hofer, F.; Aussenegg, F. R.; Krenn, J. R. *Phys. Rev. Lett.* **2005**, *95* (25), No. 257403.
(13) Akimov, A. V.; Mukherjee, A.; Yu, C. L.; Chang, D. E.; Zibrov, A. S.; Hemmer, P. R.; Park, H.; Lukin, M. D. *Nature* **2007**, *450* (7168), 402–406.
(14) Falk, A. L.; Koppens, F. H. L.; Yu, C. L.; Kang, K.; Snapp, N. D.; Akimov, A. V.; Jo, M. H.; Lukin, M. D.; Park, H. *Nat. Phys.* **2009**, *5* (7), 475–479.
(15) Li, Z. P.; Hao, F.; Huang, Y. Z.; Fang, Y. R.; Nordlander, P.; Xu, H. X. *Nano Let.t* **2009**, *9* (12), 4383–4386.
(16) Wei, H.; Ratchford, D.; Li, X. Q.; Xu, H. X.; Shih, C. K. *Nano Lett.* **2009**, *9* (12), 4168–4171.
(17) Knight, M. W.; Grady, N. K.; Bardhan, R.; Hao, F.; Nordlander, P.; Halas, N. J. *Nano Lett.* **2007**, *7* (8), 2346–2350.
(18) Fang, Y. R.; Li, Z. P.; Huang, Y. Z.; Zhang, S. P.; Nordlander, P.; Halas, N. J.; Xu, H. X. *Nano Lett.* **2010**, *10* (5), 1950–1954.
(19) Weeber, J. C.; Lacroute, Y.; Dereux, A.; Devaux, E.; Ebbesen, T.; Girard, C.; Gonzalez, M. U.; Baudrion, A. L. *Phys Rev. B* **2004**, *70* (23), No. 235406.
(20) Bozhevolnyi, S. I.; Volkov, V. S.; Devaux, E.; Laluet, J. Y.; Ebbesen, T. W. *Nature* **2006**, *440* (7083), 508–511.
(21) Neutens, P.; Van Dorpe, P.; De Vlaminck, I.; Lagae, L.; Borghs, G. *Nat. Photonics* **2009**, *3* (5), 283–286.
(22) Quinten, M.; Leitner, A.; Krenn, J. R.; Aussenegg, F. R. *Opt. Lett.* **1998**, *23* (17), 1331–1333.
(23) Economou, E. N. *Phys. Rev.* **1969**, *182* (2), 539–554.
(24) Lopez-Tejeira, F.; Rodrigo, S. G.; Martin-Moreno, L.; Garcia-Vidal, F. J.; Devaux, E.; Ebbesen, T. W.; Krenn, J. R.; Radko, I. P.; Bozhevolnyi, S. I.; Gonzalez, M. U.; Weeber, J. C.; Dereux, A. *Nat. Phys.* **2007**, *3* (5), 324–328.
(25) Bozhevolnyi, S. I.; Volkov, V. S.; Devaux, E.; Ebbesen, T. W. *Phys. Rev. Lett.* **2005**, *95* (4), No. 046802.
(26) Sanders, A. W.; Routenberg, D. A.; Wiley, B. J.; Xia, Y. N.; Dufresne, E. R.; Reed, M. A. *Nano Lett.* **2006**, *6* (8), 1822–1826.
(27) Manjavacas, A.; de Abajo, F. J. G. *Nano Lett.* **2009**, *9* (4), 1285–1289.
(28) Dickson, R. M.; Lyon, L. A. *J. Phys. Chem. B* **2000**, *104* (26), 6095–6098.
(29) Li, Z. P.; Bao, K.; Fang, Y. R.; Huang, Y. Z.; Nordlander, P.; Xu, H. X. *Nano Lett.* **2010**, *10* (5), 1831–1835.
(30) Guo, X.; Qiu, M.; Bao, J. M.; Wiley, B. J.; Yang, Q.; Zhang, X. N.; Ma, Y. G.; Yu, H. K.; Tong, L. M. *Nano Lett.* **2009**, *9* (12), 4515–4519.
(31) Goto, T.; Katagiri, Y.; Fukuda, H.; Shinojima, H.; Nakano, Y.; Kobayashi, I.; Mitsuoka, Y. *Appl. Phys. Lett.* **2004**, *84* (6), 852–854.
(32) Weeber, J. C.; Krenn, J. R.; Dereux, A.; Lamprecht, B.; Lacroute, Y.; Goudonnet, J. P. *Phys. Rev. B* **2001**, *6404* (4), No. 045411.
(33) Boltasseva, A.; Volkov, V. S.; Nielsen, R. B.; Moreno, E.; Rodrigo, S. G.; Bozhevolnyi, S. I. *Opt. Express* **2008**, *16* (8), 5252–5260.
(34) Holmgaard, T.; Chen, Z.; Bozhevolnyi, S. I.; Markey, L.; Dereux, A.; Krasavin, A. V.; Zayats, A. V. *Opt. Express* **2008**, *16* (18), 13585–13592.
(35) Pile, D. E. P.; Gramotnev, D. K. *Opt. Lett.* **2005**, *30* (10), 1186–1188.
(36) Volkov, V. S.; Bozhevolnyi, S. I.; Devaux, E.; Ebbesen, T. W. *Appl. Phys. Lett.* **2006**, *89* (14), No. 143108.
(37) Dikken, D. J.; Spasenovic, M.; Verhagen, E.; van Oosten, D.; Kuipers, L. *Opt. Express* **2010**, *18* (15), 16112–16119.
(38) Sun, Y. G.; Gates, B.; Mayers, B.; Xia, Y. N. *Nano Lett.* **2002**, *2* (2), 165–168.
(39) Wang, Z. L.; Cowley, J. M. *Ultramicroscopy* **1987**, *21* (4), 335–345.
(40) Weeber, J. C.; Dereux, A.; Girard, C.; Krenn, J. R.; Goudonnet, J. P. *Phys. Rev. B* **1999**, *60* (12), 9061–9068.
(41) Schaffer, B.; Hohenester, U.; Trugler, A.; Hofer, F. *Phys. Rev. B* **2009**, *79* (4), No. 041401.
(42) Ma, Y. G.; Li, X. Y.; Yu, H. K.; Tong, L. M.; Gu, Y.; Gong, Q. H. *Opt. Lett.* **2010**, *35* (8), 1160–1162.
(43) Tong, L. M.; Gattass, R. R.; Ashcom, J. B.; He, S. L.; Lou, J. Y.; Shen, M. Y.; Maxwell, I.; Mazur, E. *Nature* **2003**, *426* (6968), 816–819.
(44) Tong, L. M.; Lou, J. Y.; Mazur, E. *Opt. Express* **2004**, *12* (6), 1025–1035.
(45) Ditlbacher, H.; Hohenau, A.; Wagner, D.; Kreibig, U.; Rogers, M.; Hofer, F.; Aussenegg, F. R.; Krenn, J. R. *Phys. Rev. Lett.* **2005**, *95* (25), No. 257403.
(46) Dionne, J. A.; Sweatlock, L. A.; Atwater, H. A.; Polman, A. *Phys. Rev. B* **2005**, *72* (7), 075405.
(47) Chen, J.; Smolyakov, G. A.; Brueck, S. R. J.; Malloy, K. J. *Opt. Express* **2008**, *16* (19), 14902–14909.